



Combination and interpretation of $t\bar{t}$ cross section measurements with the D0 detector

The DØ Collaboration
(Dated: March 12, 2009)

We combine measurements of the top quark pair production cross section in $p\bar{p}$ collisions in the ℓ +jets, $\ell\ell$ and $\tau\ell$ final states (where ℓ is an electron or muon) at a center of mass energy of $\sqrt{s} = 1.96$ TeV in 1 fb^{-1} of data collected with the D0 detector. For a top quark mass of 170 GeV, we obtain $\sigma_{t\bar{t}} = 8.18_{-0.87}^{+0.98}$ pb. In addition, the ratios of $t\bar{t}$ cross sections in different final states are used to set upper limits on the branching fractions $B(t \rightarrow H^+b \rightarrow \tau^+\nu b)$ and $B(t \rightarrow H^+b \rightarrow c\bar{s}b)$ as a function of charged Higgs mass. Based on predictions from higher order quantum chromodynamics, we extract a mass for the top quark from the combined $t\bar{t}$ cross section.

Preliminary Results for Winter 2009 Conferences

Precise measurements of the production and decay properties of the heaviest known fermion, the top quark, provide important tests of the standard model (SM) and offer a window for searches for new physics. The inclusive top-antitop quark pair ($t\bar{t}$) production cross section ($\sigma_{t\bar{t}}$) can be measured in different $t\bar{t}$ decay channels using SM branching fractions and compared to predictions in next-to-leading order perturbative quantum chromodynamics (QCD), including higher order soft gluon resummations [1–4]. Ratios of $\sigma_{t\bar{t}}$, are particularly sensitive to new physics that may appear in top quark decays, especially if the boson from the decay is not a W boson. Additionally, many experimental uncertainties cancel in the ratios. Furthermore, the ratios An example is the decay into a charged Higgs ($t \rightarrow H^+b$), which, as predicted in some models, can compete with the SM decay $t \rightarrow W^+b$ [5]. Furthermore, since $\sigma_{t\bar{t}}$ depends on the mass of the top quark (m_t), $\sigma_{t\bar{t}}$ can be used to extract m_t . This latter measurement may be less accurate compared to direct mass measurements, but also less dependent on the top quark mass in the simulation.

Within the SM, each quark of the $t\bar{t}$ pair is expected to decay about 100% of the times into a W boson and a b quark [6]. W bosons can decay hadronically into $q\bar{q}'$ pairs or leptonically. For the latter, the decay product can be an electron and neutrino ν_e , a muon and neutrino ν_μ or a τ lepton and neutrino ν_τ , with the τ in turn decaying into an electron, a muon or hadrons (and associated neutrinos). If one of the W bosons decays hadronically while the other one produces a direct electron or muon or a secondary electron or muon from τ decay, the final state is referred to as the ℓ +jets channel. The leptonic decay of both W bosons leads to either a dilepton final state containing a pair of electrons, a pair of muons, or an electron and a muon (the $\ell\ell$ channel), or a hadronically decaying tau accompanied either by an electron or a muon (the $\tau\ell$ channel).

Here we present the combination of several measurements of $\sigma_{t\bar{t}}$, along with their ratios. From the ratios, we extract limits on the decay branching fraction of $t \rightarrow H^+b$. The combined $\sigma_{t\bar{t}}$ is also used to extract the top quark mass through a comparison with higher order QCD predictions.

Measurements of the individual $t\bar{t}$ cross sections in $\ell\ell$ and $\tau\ell$ channels using about 1 fb^{-1} of $p\bar{p}$ data from the D0 detector at the Fermilab Tevatron collider at $\sqrt{s} = 1.96 \text{ TeV}$ are available in Ref. [7]. In the ℓ +jets channel, we use the same data selection and background estimation as in Ref. [8], but an slightly larger dataset and an unified treatment of systematic uncertainties with the $\ell\ell$ and $\tau\ell$ channels. We provide below a brief summary of the event selection and analysis procedures.

In each final state we select data samples enriched in $t\bar{t}$ events by requiring one isolated high transverse momentum (p_T) lepton for the ℓ +jets channel and two for the $\ell\ell$ channel. At least two (three) high p_T jets are required for $\ell\ell$ and $\tau\ell$ (ℓ +jets) events. Further, in all but the $e\mu$ channel a large \cancel{E}_T is required to account for the large transverse momenta of neutrinos from W boson or τ lepton decays. In the $e\mu$ final state, a requirement on the sum of the leading lepton p_T and the p_T of the one or two most energetic jets is imposed instead. In the dimuon channel, the \cancel{E}_T requirement is supplemented with an \cancel{E}_T significance cut, based on probability distributions for the \cancel{E}_T and the muon and jet energy resolutions. Additional criteria are applied on the invariant mass of the two opposite charge leptons of same flavor in the ee and $\mu\mu$ channels to reduce the dominant background from $Z/\gamma^* \rightarrow \ell^+\ell^-$ decay. In the ℓ +jets and $\tau\ell$ channels we require a minimum azimuthal angle separation between the \cancel{E}_T vector and the lepton p_T [$\Delta\phi(\ell, \cancel{E}_T)$] to reduce background from multijet events. Details of lepton, jet and \cancel{E}_T identification are provided in Refs. [9, 10]. The neural-network based b -jet identification algorithm is described in Ref. [11]. The final selection in these channels demands at least one identified b jet. In the ℓ +jets channel we separate events with one or ≥ 2 b -tagged jet due to their different signal over background ratio and systematic uncertainties.

To simplify the combination and extraction of the ratios, all channels are constructed to be exclusive. If a reconstructed event can enter two selected samples, we keep it in the sample having lower statistics. This is achieved by excluding events containing any isolated electrons in the $\mu\mu$ channel, a second electron in the $e\mu$ channel, or a muon or a second electron in the e +jets channel. Because of different muon identification criteria, we reject those events from the μ +jets channel that pass the $\mu\mu$ selection or contain an electron. In the $\tau\ell$ channel we allow the signal to contain events from the ℓ +jets final state, and reject these events in the ℓ +jets channel. Finally, orthogonality between the τe channel and the $\ell\ell$ channels is achieved by rejecting events with a muon or a second electron in the τe selection. For the $\tau\mu$ channel, as in μ +jets, we reject events that pass the $\mu\mu$ selection or contain an electron.

The compositions of the samples in the $\ell\ell$, $\tau\ell$ and ℓ +jets channels are shown in Table I. W +jets production dominates the background for the ℓ +jets events, while multijet production is the most important background in the $\tau\ell$ channel. Background in the $\ell\ell$ channels comes mainly from Z +jets production. Background from diboson production is included in the column labeled “other bkg” since it is small. This column also includes the contribution from single top quark production in the ℓ +jets and $\tau\ell$ channels.

To calculate the combined cross section, we define a product function of Poisson probabilities for 14 disjoint subsamples: (i) four dilepton channels consisting of ee , $\mu\mu$ and $e\mu$ with either one or ≥ 2 jets, (ii) τe and $\tau\mu$, and (iii) eight independent ℓ +jets channels of e +jets and μ +jets, separated according to three or ≥ 4 jets, and one or ≥ 2 b -tags. Fourteen additional Poisson terms constrain the multijet background in the ℓ +jets and $\tau\ell$ channels, as determined by the number of events found in data. In particular, for the τe and $\tau\mu$ channels, the multijet background is determined by counting events with an electron or muon and associated τ of the same electric charge, introducing

TABLE I: Expected numbers of background and signal events for the measured $\sigma_{t\bar{t}}$ and observed numbers of data events. Quoted uncertainties include both statistical and systematic uncertainties.

Channel	Luminosity[pb^{-1}]	W +jets	Z +jets	Multijet	Other bkg	$t\bar{t}$	Total	Observed
e +jets (3 jets, 1 b tag)	1038	$53.4^{+6.0}_{-6.0}$	$6.0^{+1.2}_{-1.2}$	$31.5^{+3.5}_{-3.5}$	$11.4^{+1.5}_{-1.4}$	$81.7^{+6.4}_{-6.7}$	$184.0^{+9.0}_{-9.2}$	183
μ +jets (3 jets, 1 b tag)	996	$59.2^{+5.5}_{-5.6}$	$6.5^{+1.3}_{-1.3}$	$9.7^{+2.8}_{-2.8}$	$9.5^{+1.2}_{-1.2}$	$59.0^{+5.7}_{-5.6}$	$143.9^{+8.1}_{-8.1}$	133
e +jets (3 jets, ≥ 2 b tags)	1038	$5.0^{+0.8}_{-0.8}$	$0.6^{+0.2}_{-0.2}$	$2.7^{+0.3}_{-0.3}$	$2.4^{+0.4}_{-0.4}$	$30.7^{+3.9}_{-3.9}$	$41.5^{+4.7}_{-4.6}$	40
μ +jets (3 jets, ≥ 2 b tags)	996	$5.8^{+0.9}_{-0.9}$	$0.7^{+0.2}_{-0.2}$	$1.0^{+0.3}_{-0.3}$	$2.1^{+0.3}_{-0.3}$	$23.8^{+3.4}_{-3.2}$	$33.5^{+4.1}_{-3.9}$	31
e +jets (≥ 4 jets, 1 b tag)	1038	$8.5^{+2.7}_{-2.7}$	$2.2^{+0.5}_{-0.5}$	$7.9^{+1.0}_{-1.0}$	$3.0^{+0.5}_{-0.5}$	$81.6^{+8.7}_{-9.1}$	$103.3^{+7.3}_{-7.6}$	113
μ +jets (≥ 4 jets, 1 b tag)	996	$13.6^{+2.6}_{-2.7}$	$2.5^{+0.7}_{-0.6}$	$0.0^{+0.0}_{-0.0}$	$2.4^{+0.4}_{-0.4}$	$65.9^{+6.9}_{-7.2}$	$84.3^{+5.9}_{-6.3}$	99
e +jets (≥ 4 jets, ≥ 2 b tags)	1038	$1.0^{+0.3}_{-0.3}$	$0.2^{+0.1}_{-0.1}$	$1.1^{+0.1}_{-0.1}$	$0.9^{+0.2}_{-0.2}$	$41.7^{+6.0}_{-6.0}$	$44.9^{+6.0}_{-6.0}$	30
μ +jets (≥ 4 jets, ≥ 2 b tags)	996	$1.5^{+0.4}_{-0.4}$	$0.3^{+0.1}_{-0.1}$	$0.0^{+0.0}_{-0.0}$	$0.7^{+0.1}_{-0.1}$	$35.6^{+5.0}_{-5.1}$	$38.2^{+5.1}_{-5.2}$	34
ee	1074		$2.3^{+0.5}_{-0.5}$	$0.6^{+0.4}_{-0.4}$	$0.5^{+0.1}_{-0.1}$	$11.6^{+1.2}_{-1.2}$	$15.0^{+1.5}_{-1.5}$	17
$e\mu$ + 1 jet	1070		$5.5^{+0.7}_{-0.8}$	$0.9^{+0.3}_{-0.2}$	$3.1^{+0.7}_{-0.7}$	$8.9^{+1.4}_{-1.4}$	$18.4^{+1.9}_{-1.9}$	21
$e\mu$ + ≥ 2 jets	1070		$5.4^{+0.9}_{-1.0}$	$2.6^{+0.6}_{-0.5}$	$1.4^{+0.4}_{-0.4}$	$36.4^{+3.6}_{-3.6}$	$45.8^{+4.5}_{-4.5}$	39
$\mu\mu$	1009		$5.6^{+1.1}_{-1.2}$	$0.2^{+0.2}_{-0.2}$	$0.6^{+0.1}_{-0.1}$	$9.1^{+1.0}_{-1.0}$	$15.4^{+1.8}_{-1.9}$	12
$e\tau$	1038	$0.6^{+0.0}_{-0.1}$	$0.6^{+0.1}_{-0.1}$	$3.0^{+1.7}_{-1.7}$	$0.2^{+0.1}_{-0.1}$	$10.7^{+1.3}_{-1.3}$	$15.0^{+2.2}_{-2.2}$	16
$\mu\tau$	996	$0.8^{+0.1}_{-0.2}$	$1.2^{+0.3}_{-0.3}$	$8.0^{+2.8}_{-2.8}$	$0.2^{+0.0}_{-0.0}$	$12.6^{+1.4}_{-1.4}$	$22.7^{+3.2}_{-3.2}$	20

one such term per channel. In the ℓ +jets channel, we estimate the multijet background separately for each of the eight subchannels by using corresponding control data samples [12]. Four additional terms arise from applying this same method in evaluating multijet background before b -tagging.

Systematic uncertainties are included in the likelihood function through “nuisance” parameters [12], in which each independent source of systematic uncertainty is modeled by one free parameter. Each of these parameters is represented by a Gaussian probability density function with zero mean and a standard deviation (sd) of unity; all are allowed to float in the maximization of the likelihood function. Thus, the likelihood function to be maximized can be represented by the product

$$\mathcal{L} = \prod_{i=1}^{14} \mathcal{P}(n_i, \mu_i) \times \prod_{j=1}^{14} \mathcal{P}(n_j, \mu_j) \times \prod_{k=1}^K \mathcal{G}(\nu_k; 0, 1), \quad (1)$$

where $\mathcal{P}(n, \mu)$ is the Poisson probability to observe n events given the expectation of μ events. The predicted number of events in each channel is the sum of the predicted background and expected $t\bar{t}$ events, which depends on $\sigma_{t\bar{t}}$. In the product, i runs over the subsamples, and j runs over the multijet background subsamples. $\mathcal{G}(\nu_k; 0, 1)$ are the Gaussian distributions for the systematic uncertainties, where K is the total number of independent sources of systematic uncertainty, and the ν_k are the individual nuisance parameters. Each nuisance parameter is multiplied by the uncertainty (± 1 sd) calculated for each individual channel, which can affect selection efficiencies, b -tagging probabilities, theoretical cross sections, and other sources of systematics within their uncertainties, thereby changing the central value of the measured $\sigma_{t\bar{t}}$. Correlations are taken into account in a natural way, by using the same nuisance parameter for the same source of systematic uncertainty in different channels.

Systematic uncertainties on the measured $\sigma_{t\bar{t}}$ are evaluated from sources that include electron and muon identification; τ and jet identification and energy calibration; b -jet identification; modeling of triggers, signal and background; and calculated luminosity. All these uncertainties are treated as fully correlated among channels and between signal and background. Systematic uncertainties arising from limited statistics of data or Monte Carlo samples used in estimating signal or backgrounds are considered to be uncorrelated. A detailed discussion on systematic uncertainties is given in the corresponding paper [7, 8].

Table III summarizes $\sigma_{t\bar{t}}$ obtained for individual channels. Within uncertainties, all measurements are compatible with each other. The combined cross section for ℓ +jets, $\ell\ell$ and $\tau\ell$ final states for a top quark mass of 170 GeV is evaluated to be

$$\sigma_{t\bar{t}} = 8.18^{+0.98}_{-0.87} \text{ pb}, \quad (2)$$

in agreement with theory predictions [1–4]. Table II shows a breakdown of the obtained uncertainties. We evaluate the effect from each source by setting all uncertainties to zero except the one in question and redoing the likelihood maximization with respect to only that nuisance parameter. Since the method allows each uncertainty to change the

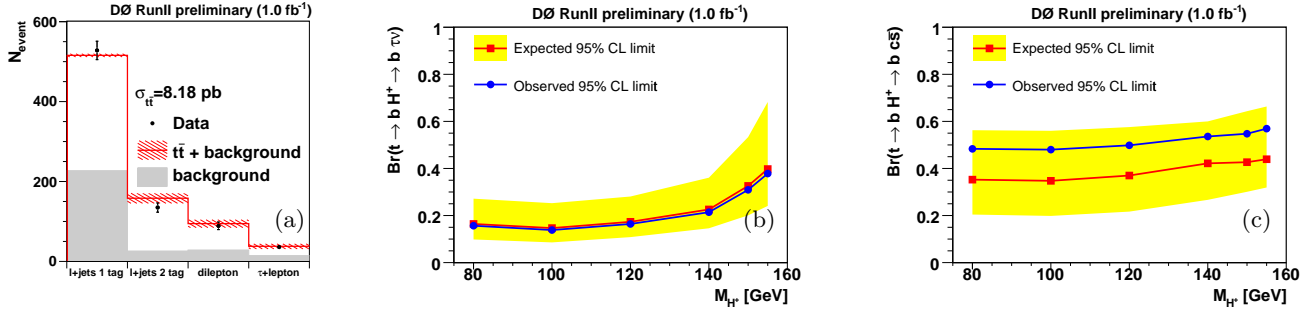


FIG. 1: Expected and observed numbers of events versus channel, used in measuring the combined $\sigma_{t\bar{t}}$ (a). Upper limits on $B(t \rightarrow H^+b)$ for tauonic (b) and leptophobic (c) H^+ decays. The yellow band shows the ± 1 sd band around the expected limit.

central value, the total uncertainty on $\sigma_{t\bar{t}}$ differs slightly from the quadratic sum of the statistical and individual systematic uncertainties. The total systematic uncertainty on $\sigma_{t\bar{t}}$ exceeds the statistical contribution. The luminosity uncertainty of 6.1% which enters into the estimation of the majority of the backgrounds and the luminosity of the selected samples is the dominant source of systematic uncertainty.

TABLE II: Summary of uncertainties on combined $\sigma_{t\bar{t}}$.

Source	$\Delta\sigma_{t\bar{t}}$ (pb)
Statistical only	+0.47 -0.46
Lepton identification	+0.15 -0.14
Tau identification	+0.02 -0.02
Jet identification	+0.11 -0.11
Jet corrections	+0.19 -0.16
Tau energy scale	+0.02 -0.02
Trigger modeling	+0.11 -0.07
b jet identification	+0.34 -0.32
Signal modeling	+0.17 -0.15
Background estimation	+0.14 -0.14
Multijet background	+0.12 -0.12
Luminosity	+0.56 -0.48
Other	+0.15 -0.14
Total systematic uncertainty	+0.78 -0.69

The observed number of events in each channel is compared to the sum of the background and combined $t\bar{t}$ signal in Fig. 1(a).

TABLE III: Summary of measured $\sigma_{t\bar{t}}$ in different channels for $m_t = 170$ GeV.

Channel	$\sigma_{t\bar{t}}$ (pb)
ℓ +jets	$8.46^{+1.09}_{-0.97}$
$\ell\ell$ [7]	$7.46^{+1.60}_{-1.37}$
ℓ +jets and $\ell\ell$	$8.18^{+0.99}_{-0.87}$
$\tau\ell$ [7]	$7.77^{+2.90}_{-2.47}$
ℓ +jets $\ell\ell$ and $\tau\ell$	$8.18^{+0.98}_{-0.87}$

We compute ratios R_σ of measured cross sections $R_{\ell\ell/\ell j} = \frac{\sigma(t\bar{t})_{\ell\ell}}{\sigma(t\bar{t})_{\ell+jets}}$ and $R_{\tau\ell/\ell\ell-j} = \frac{\sigma(t\bar{t})_{\tau\ell}}{\sigma(t\bar{t})_{\ell+jets\&\ell\ell}}$, by generating pseudo datasets around the independently measured $\sigma_{t\bar{t}}$ for the final states in the numerators and denominators. The pseudo datasets are created by variation of the signal and background around the expected number according to Poisson probabilities. All independent sources of systematic uncertainties are varied within a Gaussian distribution. Although the considered final states are exclusive, the different decay chains do not exclusively result in a given final

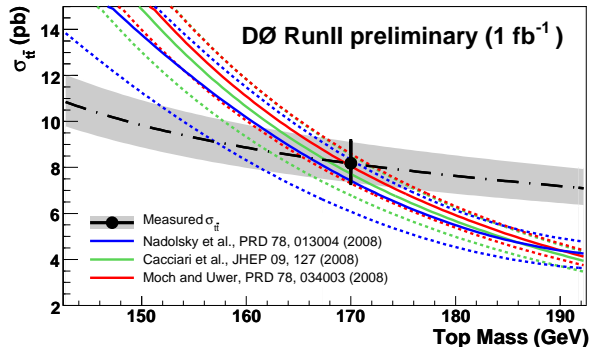


FIG. 2: Experimental and theoretical [1–3] $\sigma_{t\bar{t}}$ as function of m_t . The point shows the measured combined $\sigma_{t\bar{t}}$ the black dashed line the fit with Eq. 3 and the grey band the corresponding total experimental uncertainty.

state selection. We take into account the contribution of signal from dilepton into the ℓ +jets final state as well as the dilepton and ℓ +jets into the $\tau\ell$ channel by using the corresponding observed individual cross sections in generating the pseudo datasets. For each pseudo dataset, we perform the maximization of Eq. 1 separately in the numerator and denominator, and divide the obtained results by each other.

We obtain $R_{\ell\ell/\ell j} = 0.86^{+0.19}_{-0.17}$ and $R_{\tau\ell/\ell\ell-\ell j} = 0.97^{+0.32}_{-0.29}$, which is consistent with the SM expectation of $R_\sigma = 1$.

We use these ratios to extract upper limits on the branching ratio $B(t \rightarrow H^+b)$. In particular, a charged Higgs boson decaying into a tau and a neutrino results in more events in the $\tau\ell$ channel, while fewer events appear in the $\ell\ell$ and ℓ +jets final states compared to the SM prediction. In case of the leptophobic ($H^+ \rightarrow c\bar{s}$) model, a faster decrease of events in the dilepton compared to the ℓ +jets channel takes place for increasing $B(t \rightarrow H^+b)$. We therefore use $R_{\ell\ell/\ell j}$ to set limits on the leptophobic model, while $R_{\tau\ell/\ell\ell-\ell j}$ is explored to search for decays in which the charged Higgs bosons are assumed to decay exclusively to taus.

To extract the limits, we generate pseudo datasets assuming different branching fractions $B(t \rightarrow H^+b)$. The signal for a charged Higgs boson is simulated using the PYTHIA Monte Carlo event generator [13], and includes decays of $t\bar{t} \rightarrow W^+bH^-\bar{b}$ (and its charge conjugate) and $t\bar{t} \rightarrow H^+bH^-\bar{b}$. For a given branching fraction B , we calculate the expected number of $t\bar{t}$ events per final state,

$$N_{t\bar{t}} = [(1-B)^2 \cdot \epsilon_{t\bar{t} \rightarrow W^+bW^-\bar{b}} + 2B(1-B) \cdot \epsilon_{t\bar{t} \rightarrow W^+bH^-\bar{b}} + B^2 \cdot \epsilon_{t\bar{t} \rightarrow H^+bH^-\bar{b}}] \sigma_{t\bar{t}} L,$$

adding this to the expected background and treating the sum as a new number of expected events in each channel. We then perform the likelihood maximization to extract $\sigma_{t\bar{t}}$ from these pseudo data as if it contained only SM $t\bar{t}$ production. This provides different distributions for the ratios of cross sections for each generated B , which are compared to the observed ratio. We set limits on B by using the frequentist approach by Feldman and Cousins [14].

The observed and expected (i.e., for $R_\sigma=1$) limits for the tauonic and the leptophobic charged Higgs models are shown in Figs. 1b and 1c, respectively. From $R_{\tau\ell/\ell\ell-\ell j}$ we extract upper limits on B ranging from 15% to 40% for charged Higgs masses between 80 GeV and 155 GeV. The branching ratio B for leptophobic decays of charged Higgs from $R_{\ell\ell/\ell j}$ is smaller than 57% for the same range of charged Higgs masses.

The interpretation of the top quark mass in terms of its renormalization scheme has become a subject of intense theoretical discussion, as the uncertainty on the mass of the top quark [15] has started to approach 1 GeV, surpassing the goals of Run II at the Tevatron [16]. The extraction of this parameter from the measured cross section provides complementary information, with different sensitivity to theoretical and experimental uncertainties relative to direct methods that rely on kinematic details of the reconstruction of the top quarks. Using simulated samples of $t\bar{t}$ events generated at different values of the top quark mass, with a dependence resulting from the difference in selection efficiencies, we fit $\sigma_{t\bar{t}}$ as a function of m_t :

$$\sigma_{t\bar{t}} = \frac{1}{m_t^4} [a + b(m_t - m_0) + c(m_t - m_0)^2 + d(m_t - m_0)^3] \quad (3)$$

and obtain $a = 6.82350 \times 10^9$, $b = 1.10480 \times 10^8$, $c = 8.80552 \times 10^5$ and $d = -1.767 \times 10^3$, where $\sigma_{t\bar{t}}$ and m_t are in pb and GeV, respectively, and $m_0 = 170$ GeV.

We compare this parametrization from the combined measurement to a prediction in pure next-to-leading-order (NLO) QCD [1], to a calculation including NLO QCD and all higher-order soft-gluon resummations in next-to-leading logarithms (NLL) [2], to an approximation to the next-to-next-to-leading-order (NNLO) QCD cross section

that includes all next-to-next-to-leading logarithms (NNLL) relevant in NNLO QCD [3], and to a calculation that employs full kinematics in the double differential cross section beyond NLL using the soft anomalous dimension matrix to calculate the soft-gluon contributions at NNLO [4]. Figure 2 shows the experimental and the theoretical [1–3] $t\bar{t}$ cross sections as a function of the top quark mass.

Following the method of Refs. [7, 8], we extract top quark mass values at the 68% C.L. Since the theoretical calculations are performed in the pole mass scheme, this defines the extracted parameter here. The results are given in Table IV. All values are in good agreement with the current world average of 172.4 ± 1.2 GeV [15].

TABLE IV: Top quark mass at 68% CL for different theoretical computations of $\sigma_{t\bar{t}}$. Combined experimental and theoretical uncertainties are shown.

Theoretical computation	m_t (GeV)
NLO [1]	$165.5^{+6.1}_{-5.9}$
NLO+NLL [2]	$167.5^{+5.8}_{-5.6}$
approximate NNLO [3]	$169.1^{+5.9}_{-5.2}$
approximate NNLO [4]	$168.2^{+5.9}_{-5.4}$

In summary, we have combined the $t\bar{t}$ cross section measurements in ℓ +jets, $\ell\ell$ and $\tau\ell$ channels to measure $\sigma_{t\bar{t}} = 8.18^{+0.98}_{-0.87}$ pb for a top quark mass of 170 GeV. We have also calculated ratios of cross sections and interpreted them in terms of limits on non-standard top quark decays into a charged Higgs boson. All results are in good agreement with the SM expectations. Finally, using different theoretical calculations given in the pole mass scheme, we have extracted the top quark mass from the combined $\sigma_{t\bar{t}}$ and have found the result to be consistent with the world average top quark mass [15] from direct measurements.

We thank the staffs at Fermilab and collaborating institutions, and acknowledge support from the DOE and NSF (USA); CEA and CNRS/IN2P3 (France); FASI, Rosatom and RFBR (Russia); CNPq, FAPERJ, FAPESP and FUNDUNESP (Brazil); DAE and DST (India); Colciencias (Colombia); CONACyT (Mexico); KRF and KOSEF (Korea); CONICET and UBACyT (Argentina); FOM (The Netherlands); Royal Society and STFC (United Kingdom); MSM and GACR (Czech Republic); CRC Program, CFI, NSERC and WestGrid Project (Canada); BMBF and DFG (Germany); SFI (Ireland); The Swedish Research Council (Sweden); CAS and CNSF (China); and the Alexander von Humboldt Foundation (Germany).

-
- [1] P. M. Nadolsky *et al.*, Phys. Rev. D **78** 013004 (2008); W. Beenakker *et al.*, Phys. Rev. D **40**, 54 (1989).
 - [2] M. Cacciari *et al.*, JHEP **09**, 127 (2008); M. Cacciari, private communications.
 - [3] S. Moch and P. Uwer, Phys. Rev. D **78**, 034003 (2008); S. Moch and P. Uwer, private communications.
 - [4] N. Kidonakis and R. Vogt, Phys. Rev. D **78**, 074005, (2008); N. Kidonakis, private communications.
 - [5] J. Guasch, R. A. Jimenez and J. Sola, Phys. Lett. B **360**, 47 (1995).
 - [6] C. Amsler *et al.* [Particle Data Group], Phys. Lett. B **667**, 1 (2008).
 - [7] V. M. Abazov *et al.* [D0 Collaboration], submitted to Phys. Lett. B., arXiv:0901.2137 [hep-ex].
 - [8] V. M. Abazov *et al.* [D0 Collaboration], Phys. Rev. Lett. **100**, 192004 (2008).
 - [9] V. M. Abazov *et al.* [D0 Collaboration], Phys. Rev. D **76**, 092007 (2007).
 - [10] V. M. Abazov *et al.* [D0 Collaboration], Phys. Rev. D **76**, 052006 (2007).
 - [11] T. Scanlon, Ph.D. thesis, University of London (2006).
 - [12] V. M. Abazov *et al.* [D0 Collaboration], Phys. Rev. D **74**, 112004 (2006).
 - [13] T. Sjöstrand *et al.*, Comput. Phys. Commun. **135** 238 (2001).
 - [14] G. Feldman and R. Cousins, Phys. Rev. D **57**, 3873 (1998).
 - [15] The Tevatron Electroweak Working Group for the CDF and D0 Collaborations, arXiv:0808.1089 [hep-ex] (2008).
 - [16] A. H. Hoang and I. W. Stewart, Nucl. Phys. Proc. Suppl. **185**, 220 (2008).